The Plant Cell, Vol. 31: 1141–1154, May 2019, www.plantcell.org © 2019 ASPB.

The Chromatin-Associated Protein PWO1 Interacts with Plant Nuclear Lamin-like Components to Regulate Nuclear Size[OPEN]

Pawel Mikulski,[a,b,1,2] Mareike L. Hohenstatt,[b,1] Sara Farrona,[b,3] Cezary Smaczniak,[c,d] Yvonne Stahl,[b] Kalyanikrishna,[a] Kerstin Kaufmann,[c,d] Gerco Angenent,[d] and Daniel Schubert[a,b,4]

[a] Institute for Biology, Freie Universität Berlin, Berlin 14195, Germany
[b] Institute for Biology, Heinrich-Heine-University Düsseldorf, Düsseldorf 40225, Germany
[c] Institute for Biology, Humboldt-University Berlin, Berlin 10115, Germany
[d] Laboratory of Molecular Biology, Wageningen University, Wageningen 6700 AP, The Netherlands

ORCID IDs: 0000-0002-8899-6062 (P.M.); 0000-0002-5931-2311 (M.L.H.); 0000-0002-6855-2237 (S.F.); 0000-0002-4663-8275 (C.S.); 0000-0002-7543-5186 (Y.S.); 0000-0002-8026-246X (K.); 0000-0001-7960-6256 (K.K.); 0000-0003-4051-1078 (G.A.); 0000-0003-2390-0733 (D.S.)

Spatial organization of chromatin contributes to gene regulation of many cellular processes and includes a connection of chromatin with the nuclear lamina (NL). The NL is a protein mesh that resides underneath the inner nuclear membrane and consists of lamins and lamina-associated proteins. Chromatin regions associated with lamins in animals are characterized mostly by constitutive heterochromatin, but association with facultative heterochromatin mediated by Polycomb-group (PcG) proteins has been reported as well. In contrast with animals, plant NL components are largely not conserved and NL association with chromatin is poorly explored. Here, we present the connection between the lamin-like protein, CROWDED NUCLEI1 (CRWN1), and the chromatin- and PcG-associated component, PROLINE-TRYPTOPHANE-TRYPTOPHANE-PROLINE INTERACTOR OF POLYCOMBS1, in Arabidopsis (*Arabidopsis thaliana*). We show that PWO1 and CRWN1 proteins associate physically with each other, act in the same pathway to maintain nuclear morphology, and control expression of a similar set of target genes. Moreover, we demonstrate that transiently expressed PWO1 proteins form foci located partially at the subnuclear periphery. Ultimately, as CRWN1 and PWO1 are plant-specific, our results argue that plants might have developed an equivalent, rather than homologous, mechanism of linking chromatin repression and NL.

INTRODUCTION

Spatial organization of chromatin in the nucleus is nonrandom and contributes to gene regulation for many cellular processes (Van Bortle and Corces, 2012). Spatial organization can be categorized into several layers (Gibcus and Dekker, 2013). For instance, early cytological studies in plants showed that a subset of chromatin (heterochromatin) is densely packed and constitutes distinguishable structures called "chromocenters" (Fransz et al., 2002). Heterochromatin can be either constitutive or facultative, thus either be very stable or forming in a cell-type–dependent or cue-dependent manner. Further cytological developments revealed that interphase chromosomes occupy topological spaces in the nucleus and form distinct entities known as "chromosome territories" (Lichter et al., 1988). Moreover, chromatin conformation capture methods proved the abundance of long- and short-range genome loops, which have essential roles in gene transcription and coregulation (Kadauke and Blobel, 2009). Another aspect is the distribution of the chromatin in the interior and periphery of the nucleus (Gordon et al., 2015).

The nuclear periphery is a subnuclear space in the vicinity to the nuclear envelope (NE), a double lipid bilayer forming inner and outer nuclear membrane, and nuclear lamina (NL), a nuclear protein mesh physically associated with the inner nuclear membrane. In mammals, the NL comprises lamin-associated membrane proteins and lamins themselves, the latter being categorized as A- and B-type, depending on the structural properties and expression pattern (Dechat et al., 2010). Interestingly, lamin proteins bind specific, nonrandom regions of the chromatin and form lamina-associated domains (LADs) in animals, that are present either constitutively or form in specific cell-types (facultative LADs; Meuleman et al., 2013). LADs are generally gene-poor, associate with constitutive heterochromatin, and genes residing in LADs show no or low transcriptional activity. LADs themselves possess several features of heterochromatin—they overlap with regions that replicate late in s-phase and are enriched in repressive histone marks of histone H3 Lys-9 di/trimethylation (H3K9me2/3) and, at LAD boundaries, in H3K27me3 (van Steensel and Belmont, 2017). H3K27me3 may not overlap with LADs, but be associated with highly structured regions between LADs (Vieux-Rochas et al., 2015) and particularly assemble with lamin A, which is also present in the nuclear interior (Cesarini et al., 2015).

H3K27me3 is established by a complex of the highly-conserved Polycomb-group (PcG) proteins known as Polycomb Repressive

[1] These authors contributed equally to this article.
[2] Present address: Department of Cell and Developmental Biology, John Innes Centre, Norwich NR4 7UH, United Kingdom.
[3] Present address: School of Natural Sciences, National University of Ireland, Galway H91 TK33, Ireland.
[4] Address correspondence to: dan.schubert@fu-berlin.de.
The author responsible for distribution of materials integral to the findings presented in this article in accordance with the policy described in the Instructions for Authors (www.plantcell.org) is: Daniel Schubert (dan.schubert@fu-berlin.de).
[OPEN]Articles can be viewed without a subscription.
www.plantcell.org/cgi/doi/10.1105/tpc.18.00663

IN A NUTSHELL

Background: DNA is wrapped around histone proteins forming a structure called chromatin. The cell nucleus contains regions of chromatin that are either active or repressive, so correlated with high or low transcription, respectively. Many of those regions are dynamically regulated and switch from one state to the other under developmental cues, stress responses and cell differentiation. Repressive and active chromatin regions are largely intertwined in subnuclear space, resembling a bowl of multicolour spaghetti.

Question: At the first glance, organization of chromatin in the nucleus looks rather chaotic; however, chromatin switches are fine-tuned and specific to particular regions. How does the cell establish a given chromatin state in 3D subnuclear space? We wanted to explore that problem by studying previously uncharacterized connection between a repressive chromatin regulator and the component of nuclear periphery.

Findings: We observed that a chromatin regulator PWWP INTERACTOR OF POLYCOMBS1 (PWO1) interacts physically (via protein-protein interaction) with a structural component of the nuclear periphery CROWDED NUCLEI 1 (CRWN1). Such association is functional – mutating *PWO1* and/or *CRWN1* leads to structural changes in nuclear morphology and alters expression status of similar set of target genes. Moreover, we observed that PWO1 localizes to speckle- or network-like structures in plant nuclei, with the speckle-like foci being located predominantly at the nuclear periphery. Our results highlight the significance of subnuclear positioning of chromatin and its regulators, and add a new factor linking gene repression and nuclear periphery. Importantly, only a handful of such factors in all biological kingdoms is currently characterized.

Next steps: We plan to address whether the other regulators similar to PWO1 are also connected with structural components of nuclear periphery, understand what affects PWO1 subnuclear localization and investigate positioning of PWO1- and CRWN1-regulated genes.

Complex2 (PRC2; Margueron and Reinberg, 2011; Derkacheva and Hennig, 2014). A canonical form of PRC2 was initially discovered in *Drosophila melanogaster* and the core catalytic component is the methyltransferase Enhancer of zeste. PRC2 is present also in Arabidopsis (*Arabidopsis thaliana*), albeit with several components being multiplicated and partially diversified in expression pattern and set of targets. Enhancer of zeste homologs in Arabidopsis PRC2 are CURLY LEAF (CLF), MEDEA, and SWINGER (SWN).

LADs have not yet been identified in plants. A recent analysis identified the association of a plant nuclear pore component, with DNA/chromatin (Bi et al., 2017) but the extent of LADs in this data set is unclear and will require mapping of core-lamina–like associated proteins. Plants were long believed not to contain lamin homologs. Interestingly, the plant NL contains lamin-like proteins (Ciska and Moreno Díaz de la Espina, 2014), which, similarly to their animal counterparts, possess a coiled-coil protein motif and show general localization to the nuclear periphery (Gardiner et al., 2011; Ciska and Moreno Díaz de la Espina, 2014). Lamin-like genes in Arabidopsis form the plant-specific *CROWDED NUCLEI* (*CRWN*) family containing four members (*CRWN1*, *CRWN2*, *CRWN3*, and *CRWN4*). CRWN proteins are orthologs of NUCLEAR MATRIX CONSTITUENT PROTEIN1, which was initially discovered in carrot (*Daucus carota*) as matrix-associated protein localizing to the nuclear periphery (Masuda et al., 1997) that is land-plant–specific (Ciska et al., 2013). CRWN proteins were also biochemically identified from Arabidopsis nuclei: a crude NL fraction that had mesh-like structures composed of fibrous materials was isolated by nuclei isolation and removal of membranes. The subsequent mass spectrometry analyses resulted in the identification of 660 proteins including CRWN1 and CRWN4 (Sakamoto and Takagi, 2013). The most prominent phenotypes of CRWN family loss-of-function mutants are reduced nuclear size, increased nuclear DNA density, and abnormal nuclear shape, with the most pronounced effect seen in certain combinations of higher order mutants (Dittmer et al., 2007; Sakamoto and Takagi, 2013; Wang et al., 2013). Furthermore, CRWN proteins interact with other plant NE/NL components such as SAD1/UNC-84 HOMOLOGY1 (Graumann, 2014) and KAKU4 (Goto et al., 2014). Interestingly, *CRWN* genes also affect constitutive heterochromatin organization and 3D chromosome arrangement—different CRWN mutant combinations show altered chromocenter integrity (Dittmer et al., 2007; Wang et al., 2013) and single mutants of *crwn1* or *crwn4* exhibit elevated *trans*-chromosomal interactions, but unchanged contact frequency in *cis* (Grob et al., 2014). However, the exact mechanism of CRWN protein function in chromatin organization remains unknown.

In our previous work (Hohenstatt et al., 2018), we identified the Arabidopsis protein PROLINE-TRYPTOPHANE-TRYPTOPHANE-PROLINE (PWWP) INTERACTOR OF POLYCOMBS1 (PWO1) as a novel plant-specific factor associated with chromatin and PRC2. We showed that PWO1 binds histones and a wide range of histone modifications. PWO1 interacts physically with PRC2 methyltransferases (MEDEA, SWN, CLF), displays epistatic genetic interaction with CLF, controls expression of several PRC2-dependent target genes and is needed for full H3 and H3K27me3 occupancy at several PcG target genes. Importantly, we demonstrated that PWO1 changed nuclear localization of CLF in a transient system and recruited CLF to subnuclear speckles.

Here, we present a connection between PWO1 and the Arabidopsis NL-like structure, possibly linking H3K27me3-marked

chromatin and the nuclear periphery in plants. We demonstrate that PWO1 and PWO1-CLF speckles are positioned predominantly close to the nuclear periphery in *Nicotiana benthamiana* and that PWO1 localizes to subnuclear structures in stable Arabidopsis transgenic lines. We show that PWO1 interactors are enriched in the NL-like fraction and PWO1 associates with CRWN1 physically, genetically, and functionally, as they both control expression of a similar set of genes. Consequently, we uncover that PWO1 regulates nuclear size, a phenotypic trait related to NL-like structure. Taken together, our results uncover a novel function of PWO1 and provide a novel link between chromatin regulation and the subnuclear periphery in plants.

RESULTS

Detailed Analyses of PWO1 Subnuclear Localization

We previously demonstrated that PWO1 forms speckle-like foci upon inducible, transient expression in *N. benthamiana* (Hohenstatt et al., 2018). We also showed that upon coexpression in this system, CLF forms colocalizing speckles with PWO1, in contrast with the uniform nucleoplasmic signal of CLF when expressed alone (Hohenstatt et al., 2018). To further characterize the PWO1-CLF speckles, we coexpressed PWO1-GFP (green fluorescent protein) and CLF-mCherry fusion proteins in *N. benthamiana* leaves using a β-estradiol–inducible 35S promoter (i35S), and revealed recruitment of CLF to PWO1-speckles and colocalization of both proteins in speckles and the nucleoplasm (Figure 1A), as observed in Hohenstatt et al. (2018). The usage of an inducible promoter minimized the formation of overaccumulated protein aggregates. Of note, we previously demonstrated that PWO1 lacking the PWWP1 domain does not form speckles under the same conditions, indicating that the observed protein localization is not an effect of protein overexpression (Hohenstatt et al., 2018).

As a next step, we employed Förster resonance energy transfer with acceptor photobleaching (FRET-APB) to further characterize the PWO1-CLF interaction and demonstrated that FRET efficiencies for coexpressed samples are significantly higher than the negative controls (PWO1-GFP and CLF-GFP expressed without donor mCherry construct; Figure 1B). Interestingly, the FRET-APB donor signal intensity was higher in speckles than in the nucleoplasm, suggesting that PWO1 and CLF might form particularly tight interactions in the speckles (Figure 1B).

More detailed examination of PWO1 localization revealed a nonrandom pattern of subnuclear localization of the speckles as they are predominantly found close to the nuclear periphery in all nuclei (n = 13) examined (Figures 1C and 1D; Supplemental Figure 1). In addition, a small number of speckles was located in the nucleus interior or in vicinity to the nucleolus (Figure 1D).

Next, we sought to investigate PWO1 localization in transgenic Arabidopsis lines expressing PWO1-GFP from the *PWO1*

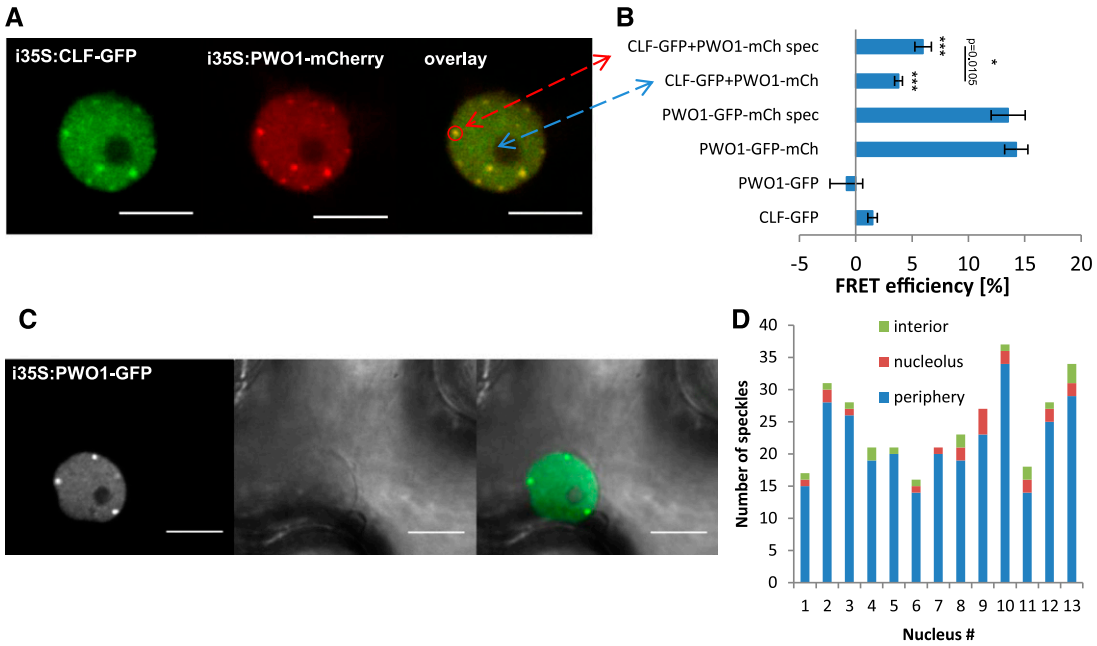

Figure 1. PWO1 Localization to Peripheral Speckles in *N. benthamiana*.

(A) A representative nucleus of *N. benthamiana* leaves coinfiltrated with i35S:CLF-GFP and i35S:PWO1-mCherry. Leaves of *N. benthamiana* were infiltrated with estradiol-inducible constructs. The images of epidermis nuclei were acquired 16 to 20 h postinduction. Scale bar = 10 μm.
(B) FRET-APB measurements for nuclei exemplified in **(A)**. FRET was measured for speckles (spec, red arrow) and diffuse localization (blue arrow). An average of efficiencies for n = 15 to 22 nuclei is shown. As positive control, a PWO1-GFP-mCherry and as negative controls, CLF-GFP and PWO1-GFP were measured. Significance level was measured using Student's t test and is represented by the asterisks: $^{*}P < 0.05$; $^{**}P < 0.01$, $^{***}P < 0.001$. Error bars = SD.
(C) A nucleus of *N. benthamiana* transiently expressing PWO1-GFP. The images were acquired and processed like in **(A)**. Scale bar = 10 μm.
(D) Number of speckles and their localization per individual nucleus.

promoter (*PWO1:PWO1-GFP*). When conventional confocal microscopy did not result in sufficient detail and resolution, we performed super-resolution microscopy (using AiryScan technology; Zeiss) in different root layers. PWO1 localized to the nucleoplasm and subnuclear structures in cortex and epidermis tissues of the root meristematic zone (Figure 2). However, the nature and detailed position of the structures remain unclear, but is clearly not entirely at the nuclear periphery. Interestingly, imaging of nuclei from the epidermis and cortex of root elongation zone revealed more uniform nucleoplasmic distribution, implying a tissue-specific pattern of PWO1 localization.

Overall, we showed that PWO1 localization, in both the transient expression system and stable Arabidopsis line, is not uniform and involves formation of foci in *N. benthamiana*, which are predominantly localized at the nuclear periphery. In our transient system, we also demonstrated that PWO1 strongly recruits CLF to peripheral speckles in the nucleus, possibly indicating that PWO1 might serve as a bridging link between the plant PRC2 and the NE.

PWO1 Physically Associates with NL/NE Proteins

Given the partially peripheral localization of PWO1, we sought to decipher the connection between PWO1 and the NE by searching for PWO1 protein interactors. We conducted coimmunoprecipitation (CoIP) experiments coupled with MS using the *PWO1:PWO1-GFP* Arabidopsis transgenic line. The protein abundance was scored via label-free quantification analysis, and a comparison to background sample (Col-0, wild type) was used to identify significantly enriched proteins in the *PWO1:PWO1-GFP* line. As a result, we obtained a list of 99 putative PWO1 interactors.

Consistently with the chromatin- and PcG-related role of PWO1 (Hohenstatt et al., 2018), we detected other proteins with similar functions (Figure 3A; Supplemental Table 1). Those included TELOMERE REPEAT BINDING1 (TRB1), belonging to the TRB family that recruits core PcG proteins to DNA via recognition of telobox *cis*-regulatory motifs (Zhou et al., 2016); YING YANG1, a transcription factor corepressing plant disease susceptibility genes (Lai et al., 2014) and Arabidopsis putative ortholog of the animal PRC2 recruiter YING YANG1/Pleiohomeotic (Atchison et al., 2003); AT1G79020, an ortholog of Enhancer of Polycomb-like proteins and an interactor of NuA4 and SWR1-C complexes responsible for histone acetylation and histone variant exchange (Bieluszewski et al., 2015); PWWP domain protein3, which is found in a complex with PcG proteins (Zhou et al., 2018); and MSI1, an Arabidopsis PRC2 component (Hennig and Derkacheva, 2009). PWO1 did not precipitate other PRC2 members, suggesting that the physical interaction of PWO1 with several PRC2 components may be transient or not very stable. Moreover, PWO1 immunoprecipitated various components of chromatin remodeling complexes, such as CHROMATIN REMODELING12 and 17, ACTIN RELATED PROTEIN4, AtBAF60/AtSWP73B/CHC1, and SWITCH/SUCROSE NONFERMENTING3A. These results are in agreement with PWO1's putative role in controlling nucleosome occupancy and decreased histone H3 enrichment in *pwo1* at several PcG targets (Hohenstatt et al., 2018). In addition, PWO1 coprecipitated various histone proteins, confirming the previously shown in vitro interactions with histone H3. Lastly, we discovered that PWO1 is associated with members of the PEAT-complex

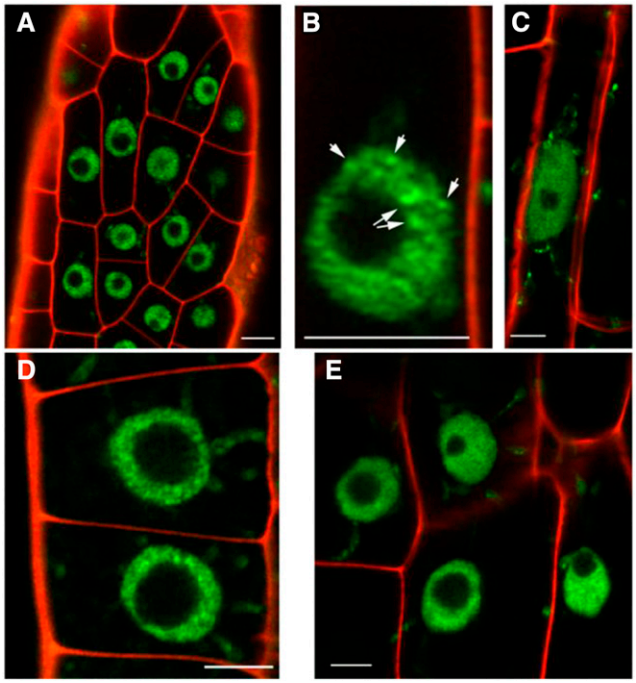

Figure 2. PWO1 Localization in Arabidopsis.

Super-resolution microscopy images (LSM880 AiryScan; Zeiss) from roots of PWO1:PWO1-GFP. The images represent nuclei from the meristematic zone epidermis in an overview **(A)** and or zoomed in **(B)**, elongation zone epidermis **(C)**, meristematic zone cortex **(D),** and elongation zone cortex **(E)**. "Black holes" are nucleoli. Cells were counterstained with Propidiumiodide (red). The most prominent subnuclear structures are marked with arrows. Scale bars = 5 μM.

(PWWP domain-containing proteins-Enhancer of Polycomb-Related [EPL]-AT-rich interaction domain-containing proteins [ARID]-telomere repeat binding proteins [TRB] complex), which was recently identified to silence transposable elements (Tan et al., 2018).

Interestingly, we discovered that ~56% of PWO1 putative interactors (55 of 98 proteins) overlap with the components of a crude plant NL-like fraction (Figure 3B; Sakamoto and Takagi, 2013), including constitutive NL/NE members, such as CRWN1, CRWN4, and SAD1/UNC-84 DOMAIN PROTEIN 1. The overlap contained also chromatin-associated proteins, like SKI-INTERACTING PROTEIN1, CHROMATIN REMODELING17, ACTIN RELATED PROTEIN4, AtBAF60/CHC1, and MSI1 (Figure 3B; Supplemental Table 1). However, PEAT complex members, which include PWO1, PWO2, and PWO3, are not identified in the NL fraction (Tan et al., 2018). Overall, the high number of PWO1 interactors overlapping with the NL fraction is in agreement with the presence of PWO1 speckles at the nuclear periphery, which were revealed in the transient expression experiments.

We focused further analyses on the putative interaction with CRWN1, a nuclear lamin-like protein with a prominent role in nuclear morphology (Wang et al., 2013), chromocenter (Dittmer et al., 2007), and interchromosomal contact frequency regulation (Grob et al., 2014). To detect a direct PWO1-CRWN1 interaction,

A

TAIR ID	Name	P-value	Log_2 ratio	Unique peptides	Sequence coverage [%]	Present in NL fraction?
Bait protein						
AT3G03140	PWO1	2.76E-03	21.58	17	28.7	
Constitutive NL/NE components						
AT1G67230	CRWN1	3.12E-02	3.63	3	3.4	✓
AT5G65770	CRWN4	4.13E-04	6.50	4	5.2	✓
AT5G04990	SUN1	3.54E-03	2.54	2	7.6	✓
PcG and chromatin-associated proteins						
AT5G58230	MSI1	5.13E-03	8.08	2	7.1	✓
AT1G49950	TRB1	4.23E-03	15.00	2	10.1	
AT4G06634	AtYY1	7,04E-03	11.90	3	14.0	
AT1G79020	E(Pc)	8,44E-07	4.98	2	4.6	
AT1G77180	SKIP	2.54E-03	2.84	4	8.2	✓
AT5G18620	CHR17	3.76E-03	12.04	4	4.3	✓
AT3G06010	CHR12	4.30E-03	11.41	5	5.7	
AT1G18450	ARP4	0.04	12.25	4	15	✓
AT5G64420	SWI3A	0.02	10.33	4	10.2	
AT5G14170	CHC1	1,99E-03	16.23	8	15.7	✓

B

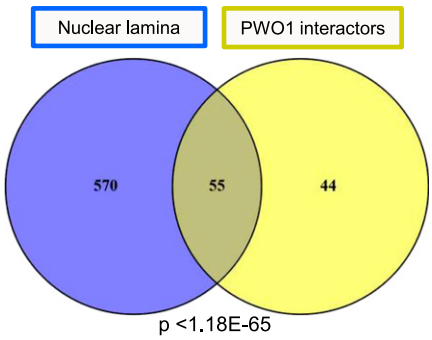

Figure 3. Identification of PWO1 Interactors.

(A) MS results for bait protein and selected PWO1 interactors. NL fraction represents proteins detected in crude NL extract.
(B) Overlap between Arabidopsis NL fraction and PWO1 interactors. PWO1 interactors correspond to proteins showing significant ($P < 0.05$) enrichment over the wild type in CoIP-MS/MS experiment. Significance level of the overlap was calculated using the Student's *t* test. For the full list of 65 overlapping proteins, see Supplemental Table 1.

we performed Yeast-Two-Hybrid (Y2H) and FRET-APB in *N. benthamiana*. Of note, in our hands, CRWN1 protein transiently expressed in *N. benthamiana* leaves showed not only NE-localization, but was also present uniformly in the nucleoplasm and caused nuclear membrane deformations, as reported in Goto et al. (2014) and Graumann (2014). Y2H and FRET-APB experiments revealed no or very low interaction between CRWN1 and full-length PWO1, but much stronger signal over negative controls when only a C-terminal PWO1 fragment (634 to 769 amino acids) was used instead (Figure 4; Supplemental Figures 2 and 3). This result might indicate steric constrains of overall PWO1 protein folding caused by introduction of fusion tags (Gal4 [GALactose metabolism4]-domains or FRET fluorophores), which may mask the CRWN1 binding site in full-length PWO1 construct versions. By contrast, the use of a truncated PWO1 protein containing the CRWN1-interacting region might resolve potential steric effects. The interaction with CRWN1 was shown to be specific to the C-terminal part of PWO1 and not a simple outcome of random binding of any truncated PWO1 versions, as the other PWO1 fragments (frag.1 and frag.2) still show a background-level interaction (Figure 4B).

Interestingly, the CRWN1-interacting region in the PWO1 sequence does not contain any annotated protein domain (Figure 4A). However, an alignment to the closest PWO1 plant homologs revealed a high level of conservation for the PWO1 C-terminal sequence in *Brassicaceae* species other than Arabidopsis (Supplemental Figure 3), highlighting a functional importance of this fragment. By contrast, the PWO1 C-terminal fragment is largely absent from PWO2 and PWO3, suggesting partially separate functions between PWO family proteins in Arabidopsis.

PWO1 Interacts Genetically with CRWN1

Given the physical association of PWO1 and CRWN1, we sought to investigate their functional connection by studying *pwo1*, *crwn1*, and *pwo1 crwn1* mutants at the phenotypic level. As PWO1 was shown to interact with PRC2 components (Hohenstatt et al., 2018), we included also *swn* and *swn crwn1* lines in our analysis to characterize the link between the NL-like structure and canonical PRC2 members.

A prominent feature of mutants of NE or NL components is the reduction in nuclear size and change of nuclear shape. To characterize alterations in nuclear morphology, we isolated nuclei from whole seedlings, stained them with 4′,6-diamidino-2-phenylindole (DAPI), and measured their nuclear area and circularity (Figure 5). Consistently with other studies (Wang et al., 2013), we observed a reduction in nuclear area and increase in circularity index in *crwn1*, compared with the wild-type control (Col-0). Interestingly, lower average nuclear area was also observed in *pwo1*, albeit with no significant changes in nuclear shape. Importantly, we detected no substantial alterations in ploidy levels in *pwo1* in comparison with the wild type (similar to results obtained

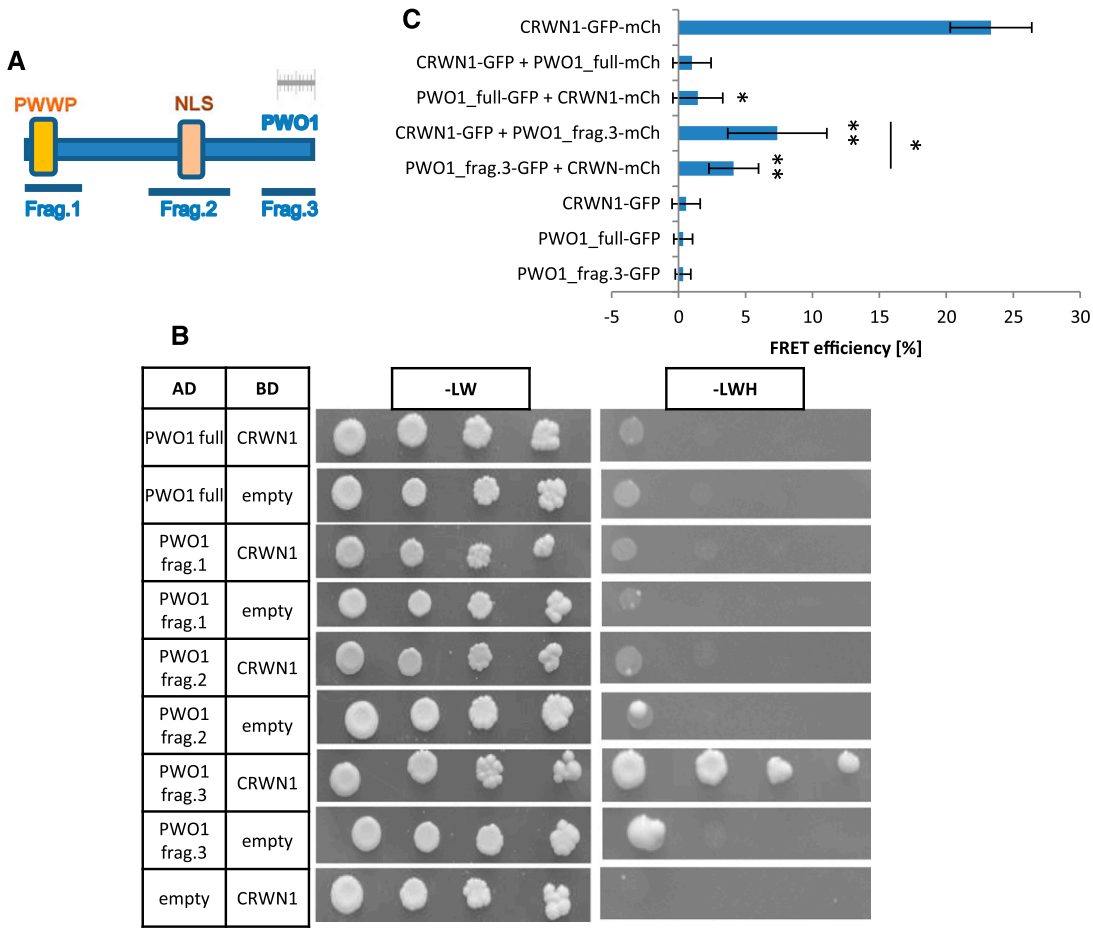

Figure 4. Analysis of PWO1-CRWN1 Interaction.

(A) Scheme of PWO1 protein with different coding sequence fragments used in **(B)** and **(C)**. NLS, predicted nuclear localization signal. Scale bar on the top of the scheme = 100 amino acids.

(B) Y2H analysis on PWO1-CRWN1 interaction. Overall yeast growth and protein interaction among CRWN1, PWO1, and PWO1 fragments was assessed on transformation medium (-LW, -Leucine Tryptophane) and selection medium (-LWH, -Leucine Tryptophane Histidine). AD, activation domain; BD, DNA-binding domain.

(C) FRET-APB-based interaction between PWO1 and CRWN1. FRET efficiency was calculated for nuclei from the positive control ($n = 10$), negative controls ($n = 15$ to 17), and interaction samples ($n = 15$ to 27). Error bars = SD values. Significance between interaction samples and their respective negative controls was inferred from Student's t test. Significance threshold: $^{*}P < 0.05$, $^{**}P < 0.01$.

for *crwn1* mutants; Dittmer et al., 2007), suggesting that changes in endoreduplication do not underlie the observed reduction in nuclear size (Supplemental Figure 4).

The analysis of *pwo1 crwn1* phenotype revealed that both genes act in the same pathway to control nuclear size as the double mutant phenocopies either of the single mutants (Figure 5B). Interestingly, we also observed a genetic interaction for the nuclear shape phenotype. As *pwo1 crwn1* shows a circularity index average similar to *pwo1*, the CRWN1-dependent nuclear shape alteration was suppressed by the lack of functional *PWO1* (Figure 5C). Consistently, we found that the nuclei from *pwo1 crwn1* are characterized by a broad distribution of circularity index levels, similarly to the *pwo1* single mutant. By contrast, the nuclei from *crwn1* are narrowly distributed and enriched at the high circularity index levels (Figure 5D). This result suggests that PWO1 is required for CRWN1-mediated control of nuclear shape.

Furthermore, we observed no significant changes in nuclear morphology in *swn*. The double mutant *crwn1 swn* showed an increased average circularity and reduced average nuclear area, hence resembling *crwn1*. Consistent with this, a distribution of individual nuclei in *crwn1 swn* is more similar to the distribution observed in *crwn1*, rather than *swn*. The phenocopy of nuclear morphology changes between *swn crwn1* and *crwn1*, yet lack of such a phenotype in *swn*, suggests that SWN does not influence nuclear architecture.

Overall, our results suggest that PWO1 and CRWN1 determine nuclear size and shape within the same genetic pathway. By contrast, a canonical PRC2 component, SWN, does not influence morphology of the nucleus, irrespective of CRWN1 function.

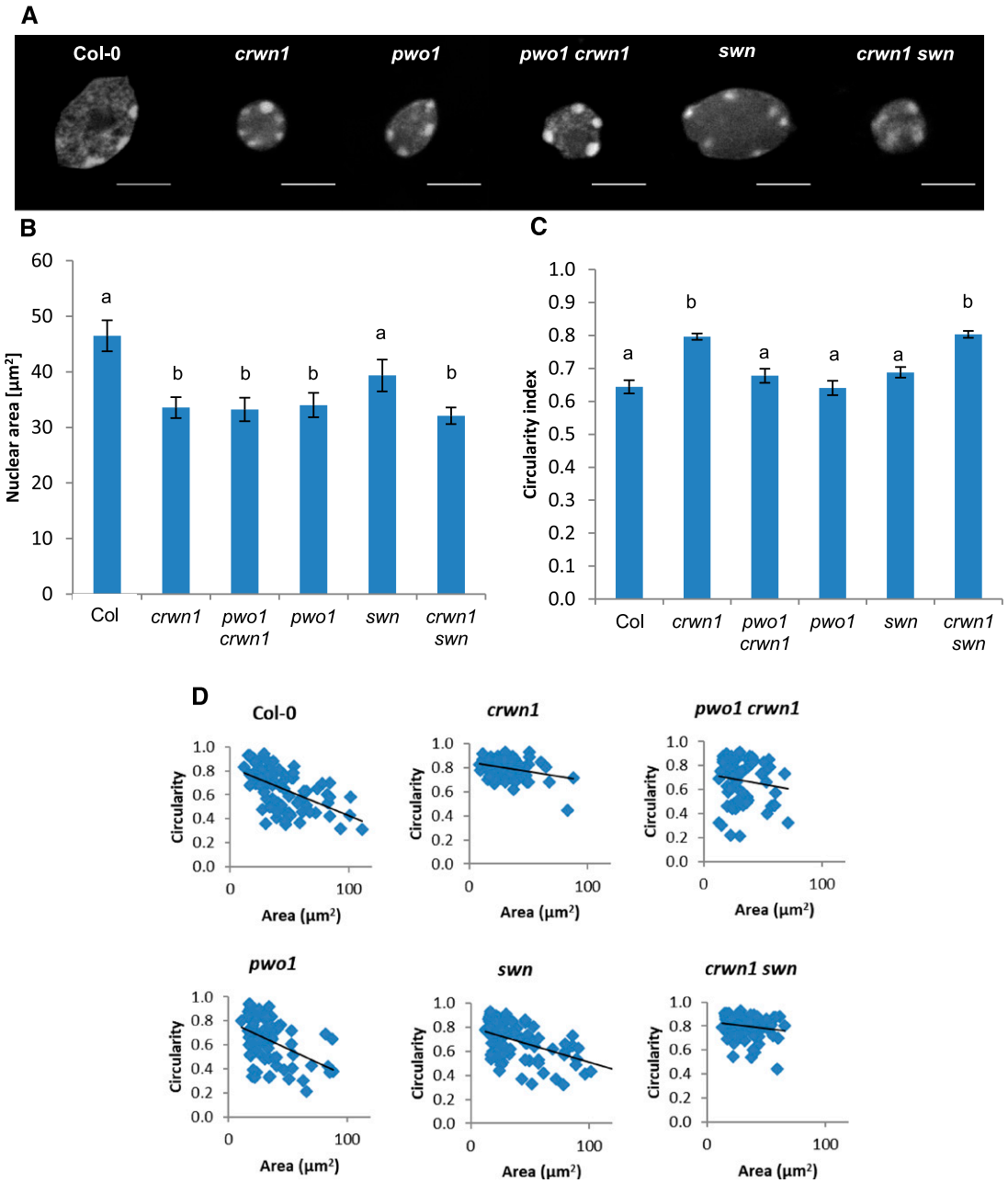

Figure 5. Genetic Interaction of *pwo1*, *crwn1*, and *swn*.

(A) DAPI-stained nuclei in different genotypes. Scale bars = 20 µm.
(B) and **(C)** Nuclear area **(B)** and circularity **(C)** measurements. Calculations were performed on Z plane showing the largest area of particular nucleus in the Z-stack. A quantity of 72 to 92 nuclei per genotype were measured. Circularity index was calculated as 4π (area/perimeter^2), with the maximal value of 1.0 corresponding to the perfect circle. Error bars are derived from standard error (SE). Significance was calculated using one-way analysis of variance followed by Student's *t* test ($P < 0.001$).
(D) The relationship between circularity index and nuclear area in nuclei from genotypes used in the study. Blue diamonds represent individual nuclei; black line displays the trendline.

Loss of *PWO1* and *CRWN1* Does Not Drastically Affect Reciprocal Localization

Given the physical and genetic interaction between PWO1 and CRWN1, we asked whether their patterns of subnuclear localization are dependent on each other. We showed that PWO1 forms foci in the meristematic zone of the Arabidopsis root. In turn, CRWN1 is known to localize exclusively to the nuclear periphery, forming a thin ring delineating the border of the nucleus (Supplemental Figure 5; Dittmer et al., 2007). However, our

confocal microscopy analyses of the lines *PWO1*:*PWO1-GFP crwn1* and *CRWN1*:*CRWN1-GFP pwo1 pwo3* revealed no obvious changes in subnuclear localization in comparison to the control lines (Supplemental Figures 5 and 6). Therefore, our results suggest that the subnuclear localizations of PWO1 and CRWN1 are either independent of each other or that only mild alterations occur, which are difficult to detect by conventional confocal microscopy.

Loss of *PWO1* and *CRWN1 CRWN2* Affect Expression of a Similar Set of Genes

To further understand the connection between *PWO1* and *CRWN* family genes, we investigated the global transcriptomic changes in seedlings of *pwo1* and *crwn1 crwn2* mutants using RNA sequencing (RNA-Seq). Given the phenotypes of *crwn1* and *crwn1 crwn2* (Dittmer et al., 2007), we decided to use the stronger double *crwn1 crwn2* mutant to depict a larger effect of CRWN family-dependent transcriptomic changes. Differential expression analysis (see "Methods") identified 179 significantly upregulated and 242 significantly downregulated differentially expressed genes (DEGs) in *pwo1*, as compared with the wild-type control (Col-0). In turn, similar analysis on *crwn1 crwn2* revealed 602 significantly upregulated and 214 significantly downregulated DEGs. Cross-comparison of the data sets from both genotypes revealed a significant overlap of 71 upregulated and 73 downregulated DEGs (Figures 6A and 6B). These results imply that *PWO1* and *CRWN1/CRWN2* regulate a partially similar set of target genes.

Next, we asked whether common DEGs affected by both *pwo1* and *crwn1/2* are associated with specific functional categories. Our gene ontology (GO) analysis (see "Materials and Methods") on the overlap of upregulated DEGs showed a significant enrichment of the functions related to response to stress (biotic and abiotic), iron homeostasis, and transport of amino acids/nitrate (Figure 6C). In turn, DEGs from the overlap of downregulated targets are involved specifically in the response to auxin.

Given PWO1's involvement in the PRC2 pathway (Hohenstatt et al., 2018), we hypothesized that upregulated DEGs in *pwo1* are covered by H3K27me3 in wild-type plants. Therefore, we compared our list of upregulated-DEGs in *pwo1* and a published data set of H3K27me3 targets (Oh et al., 2008). Indeed, we detected

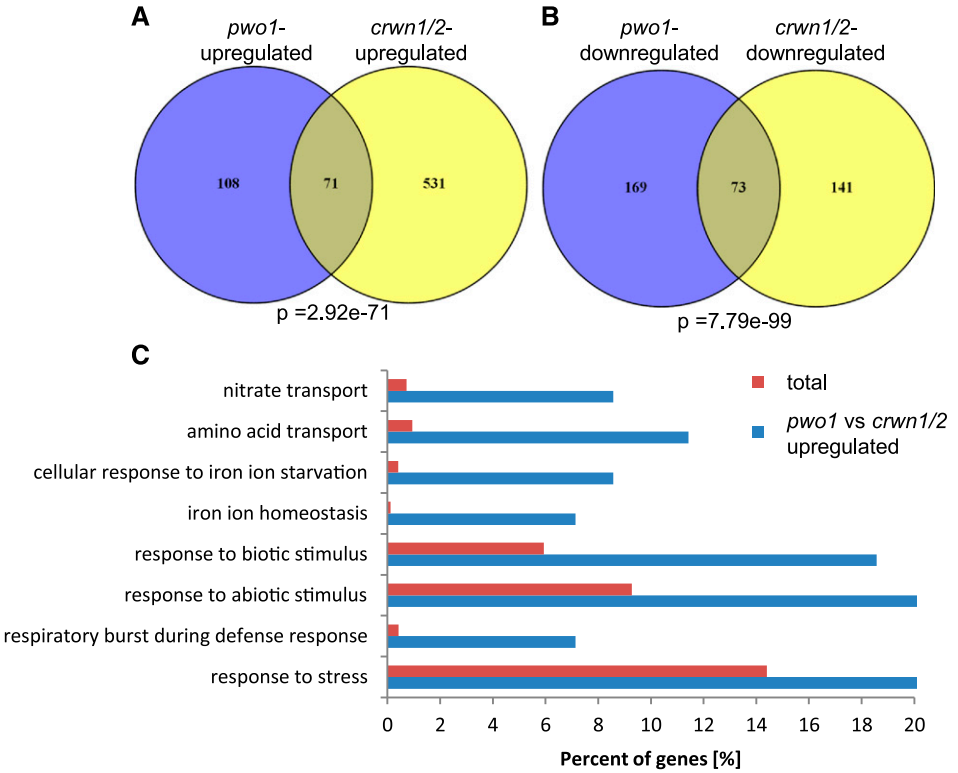

Figure 6. DEG Analysis—Overlap Between *pwo1* And *crwn1/2*.

(A) Venn diagram comparing upregulated-DEGs in *pwo1* (*pwo1*-upregulated) and *crwn1/2* (*crwn1/2*-upregulated). Significance level of the overlap was calculated in the software "R" using a hypergeometric test.

(B) Venn diagram comparing downregulated-DEGs in *pwo1* (*pwo1*-downregulated) and *crwn1/2* (*crwn1/2*-downregulated). Significance level of the overlap was calculated in the software "R" using a hypergeometric test.

(C) GO-term enrichment analysis on commonly upregulated-DEGs in *pwo1* and *crwn1/2* as compared with all TAIR10 protein-coding genes ("total"). The percentage corresponds to the number of genes enriched in significantly abundant (*FDR* < 0.005) GO terms in the overlap shown in **(A)** or the whole protein-coding gene number based on TAIR10 annotation.

a significant overlap of 105 genes present in both lists (Figure 7A), showing that PWO1 is required for the repression of a subset of PRC2 targets. As PWO1 associates with CRWN1, we asked whether mutants in the CRWN gene family affect expression of H3K27me3 targets as well. Interestingly, the comparison between upregulated DEGs in *crwn1/2* and H3K27me3-covered genes revealed a significant number of genes shared between two data sets (Figure 7A). Finally, cross-comparison of upregulated DEGs in *pwo1* and *crwn1/2*, and H3K27me3 targets gave 36 genes shared by all three data sets (Figure 7A). Their function is related to stress response and amino acid/nitrate transport, but not to iron metabolism (Figure 7B), which implicates a role of PWO1 and CRWN1 in iron homeostasis facilitated in a PRC2-independent manner. We noted also a substantial number of H3K27me3 targets whose expression is affected only by either loss of *PWO1* or *CRWN1 CRWN2*. This result suggests that PWO1 and CRWN1 mediate repression (directly or indirectly) of PRC2 targets also independent of each other.

DISCUSSION

Here, we demonstrate that the Arabidopsis chromatin- and PRC2-associated protein PWO1 interacts physically with numerous NL-like components, including CRWN1—a coiled-coil analog of lamin proteins in Arabidopsis. We report that *PWO1* and *CRWN1* are epistatic in controlling nuclear size and affect expression of a similar set of PRC2 target genes. Moreover, we show that PWO1 in *N. benthamiana* localizes to subnuclear foci, which are located mostly within the nuclear periphery. PWO1 in Arabidopsis show also a nonuniform localization in meristematic tissues; however, the features and precise subnuclear position of observed structures require further exploration. Future studies should also elucidate whether PWO1 structures in Arabidopsis are separate entities or form a large interconnected subnuclear network.

Our findings suggest a conservation of the association between a repressive chromatin environment and the nuclear periphery across biological kingdoms, including plants. Strikingly, the exact mechanism and linking factors involved in this phenomenon are frequently species-specific, as has been reported for i.e. *Caenorhabditis elegans*-specific 4 (Gonzalez-Sandoval et al., 2015) or Silent Information Regular4, present in Saccharomycetaceae only (Taddei et al., 2004; Hickman et al., 2011). Identification of PWO1, a novel plant-specific bridging factor, adds another evolutionary distinct element in an otherwise conserved machinery linking chromatin repression with NL-like structures.

The pathways linking repressive and specifically PRC2-regulated chromatin and the NL vary not only between species, but also within the same organism. Many protein effectors associated with the NL in fungi or animals regulate only a specific subset of targets and play roles also outside of the nuclear periphery (Harr et al., 2016). Consequently, our results on PWO1 subnuclear localization, transcriptomic analyses in *pwo1* and *crwn1/2*, and predominantly nucleoplasmic distribution of H3K27me3 in plants (Mathieu et al., 2005) collectively suggest a NL- and PWO1-dependent repression of only a specific set of PRC2 targets. We speculate that the other, PWO1-independent, pathways bridging the NL and PRC2 also exist, as suggested by the PWO1-independent CRWN1/2-mediated repression of PRC2 target genes. Certainly, an identification of such pathways will be the essential step for the future. The feature of altered nuclear size

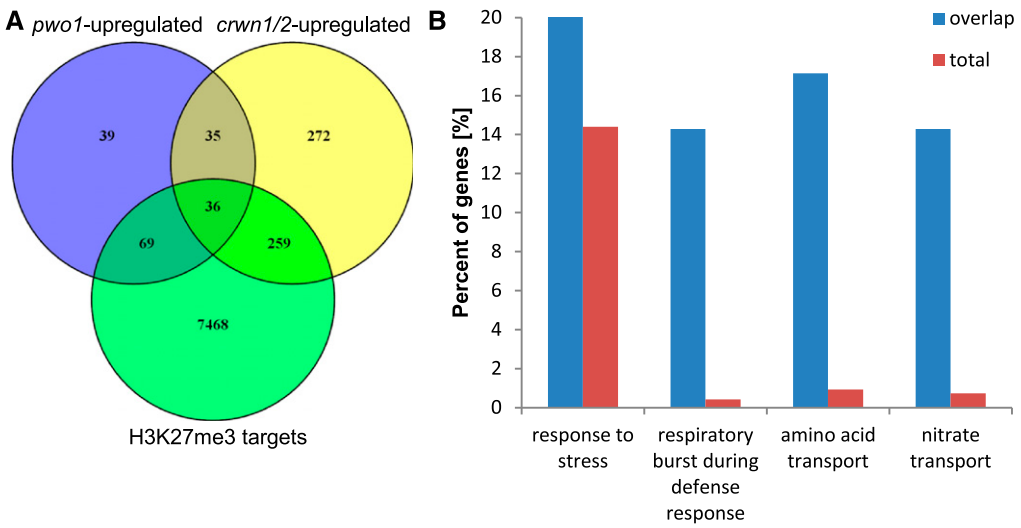

Figure 7. DEG Analysis—Cross-Comparison Between Mutants And H3K27me3 Targets.

(A) Venn diagram comparing: upregulated-DEGs in *pwo1* (*pwo1*-upregulated), in *crwn1/2* (*crwn1/2*-upregulated), and H3K27me3 targets in Col-0. The significance level of overlapping gene number is as follows: 4.56e-06 (H3K27me3 targets versus *pwo1*-upregulated), 2.20e-06 (H3K27me3 targets versus *crwn1/2*-upregulated), and 5.64e-28 (H3K27me3/*pwo1*-upregulated versus H3K27me3/*crwn1/2*-upregulated). *P* values were calculated in the software "R" by a hypergeometric test.

(B) GO-term enrichment analysis on commonly upregulated DEGs in *pwo1* and *crwn1/2*, and H3K27me3 targets in Col-0, as compared with all TAIR10 protein-coding genes ("total"). The percentage corresponds to the number of genes enriched in significantly abundant (*FDR* < 0.0005) GO terms in the common target genes shared by all three data sets in **(A)** or the whole protein-coding gene number based on TAIR10 annotation.

with unchanged endoreduplication in mutants of stable NL components (like *crwn1*) and its associated members (like *pwo1*) provides a measurable phenotype for unbiased mutagenic screens (Goto et al., 2014).

Target-specificity of NL-chromatin bridging pathways is demonstrated also by the phenotypes of respective mutants. In animals, lack of bridging factors is frequently represented by a normal viability and only mild aberrations in standard conditions, with a substantial effect seen only at selected developmental stages or environments (Ozawa et al., 2006; Towbin et al., 2012; Gonzalez-Sandoval et al., 2015). Similarly, the *pwo1* mutant shows a mild phenotype, with obvious changes known so far for one specific trait only (flowering time; Hohenstatt et al., 2018). As disruption of all PWO family members in *pwo1/2/3* displays severe effect (seedling lethality; Hohenstatt et al., 2018), we cannot exclude that the mild phenotype in *pwo1* single mutant is caused by the overlapping function of PWO family proteins. However, a nuclear area reduction seen already in *pwo1* single mutant and the absence of a conserved CRWN1-interacting motif in PWO2 and PWO3 suggests that PWO1 has a NL-connected role separate from the other PWO family members. PWO1/2/3 are part of the recently discovered PEAT complex (Tan et al., 2018), and disruption of either the ARID, the TRB, or the EPL component results in early seedlings lethality, similar to *pwo1/2/3* triple mutants (Hohenstatt et al., 2018; Tan et al., 2018). Thus, the fraction of PWO1, together with PWO2 and PWO3, present in the PEAT complex (which is not purified in the crude lamina extraction) is probably required for proper seedling growth whereas PWO1 association with NL components regulates nuclear size.

Furthermore, our results on PWO1 subnuclear localization showed formation of predominantly peripheral speckles in *N. benthamiana* and nonuniform subnuclear localization in Arabidopsis. Formation of distinguishable nucleoplasmic foci is a prominent feature of PcG proteins in animals, specifically PRC1 (Pirrotta and Li, 2012) and was reported to be dependent on PRC2 activity (Hernández-Muñoz et al., 2005). Moreover, animal H3K27me3 is found in large aggregates at the nuclear periphery when associated with late-replicating chromatin (Hernández-Muñoz et al., 2005). Similarly to animal models, PRC1 members in Arabidopsis were found to localize into multiple speckles as well (Libault et al., 2005; Calonje et al., 2008; Berry et al., 2017), albeit without any preference toward the nuclear periphery.

Our transcriptomic analyses, presented together with the nuclear size phenotype, highlight another important point. As reduced nuclear area causes elevated frequency of interchromosomal contacts (Grob et al., 2014), changes in the gene expression in *pwo1* and *crwn1/2* might reflect indirect effects coming from altered spatial organization of the chromatin. Thus, a generation and cross-comparison of transcriptomic data from the other mutants affected in nuclear size should be performed to uncouple effects of direct target regulation from the indirect effects.

In short, we provide a link between NL-like structures and chromatin repression in plants, highlighting an importance of nuclear architecture proteins in the control of gene expression across biological kingdoms. Deepening our understanding of PWO1 serves as a fascinating opportunity to decipher the mechanistic link between gene silencing and the nuclear periphery.

METHODS

Plant Material

Arabidopsis (*Arabidopsis thaliana*) seedlings were grown on 1/2-strength Murashige and Skoog plates in 16-h light/8-h dark conditions at 22°C (light intensity was 120 μmol/m^2/s using Planox Eco 451178.009 LED bulbs [RZB]; long-day [LD] conditions) and transferred to soil, when later stages of development were needed. For the knock-out mutations, the following transgenic lines were used: *pwo1-1* (SAIL_342_C09), *crwn11* (SALK_025347), *crwn1-1 crwn2-1* (SALK_025347, SALK_076653), and *swn-7* (SALK_109121). For transient assays, *Nicotiana benthamiana* plants were grown in soil in LD conditions (22°C) up to the 4th week and subsequently used for infiltration. The sequences of oligonucleotides used for genotyping are as described in Wang et al. (2013) and .

Cloning

Regarding the vectors used for FRET-APB, pMDC7 derivatives containing GFP, mCherry, and GFP+mCherry coding sequences were created as described in Bleckmann et al. (2010). Next, genomic sequence of *CRWN1* (AT1G67230), coding region of full *PWO1* sequence (AT3G03140) or coding region of PWO1 C-terminal fragment were ligated into pCR8-GW-TOPO using the TA Cloning Kit (Thermo Fisher Scientific) to create entry vectors. To construct translational fusion plasmids, insert sequences from the entry vectors were introduced into pMDC7 derivatives via Gateway reaction from the Gateway cloning protocol (Thermo Fisher Scientific). For Y2H experiments, the coding sequences of CRWN1, PWO1, and PWO1 fragments were used to create entry vectors via TA Cloning and subsequently introduced into pGADT7 and pGBKT7 Y2H vectors (Clontech) using LR reaction (Thermo Fisher Scientific).

CoIP-MS/MS

Nuclear proteins were isolated from 3 g of whole seedlings from *PWO1*:*PWO1-GFP* or Col-0 (negative control) lines grown in LD conditions. Four biological replicates per genotype were used. Nuclei were extracted without prior fixation of the tissue as described in Smaczniak et al. (2012) and the further procedure was performed as described by Smaczniak et al. (2012). For immunoprecipitation, a μMACS GFP Isolation Kit (Miltenyi Biotec) was used. Peptide spectra were obtained with a model no. LTQ Orbitrap XL Mass Spectrometer (Thermo Fisher Scientific). Protein identification was performed by database search with the Andromeda search engine (Cox et al., 2011). Raw data processing was done with the software MaxQuant (v1.1.1.36; Cox and Mann, 2008). To distinguish PWO1-interacting proteins from the background, Student's *t* test with a false discovery rate (*FDR*) adjustment was performed on label-free quantification values. For overlap between NL and PWO1 interactors, hits corresponding to chloroplastic genes were excluded from the data sets.

Subnuclear Localization and FRET-APB

For FRET-APB and examination of subnuclear localization in *N. benthamiana*, estradiol-inducible pMDC7 vector derivatives were transformed into *Agrobacterium tumefaciens* (GV3101 PMP90 strain with p19 silencing suppressor plasmid) and grown onYeast Extract Broth (YEB) medium plates for 2 d. Bacterial lawn was scraped into infiltration medium (5% [w/v] Suc, 0.1% [v/v] Silwet-L77, 450 μM of acetosyringone) to OD = 0.8 and kept on ice for 1 h. Bacteria were infiltrated into 4-week–old *N. benthamiana* leaves using 1-mL syringes without needles. After 48 h, an induction was performed by painting the abaxial side of the leaves with 20 to 50 μM of Beta-estradiol solution in 0.1% (v/v) TWEEN-20. At 16- to 20-h post-induction, small pieces of leaves around infiltration spots were cut,

mounted on the microscopic slides, and subjected to confocal microscopy on a LSM780 (Zeiss) or SP8 (Leica). High-quality images were acquired with 3- to 4-line averaging and their brightness was adjusted in the software FIJI/ImageJ (National Institutes of Health).

The vicinity of speckles to the nuclear periphery or nucleolus was inferred from the distance between border of the speckle/the border of GFP nucleoplasmic signal and a nuclear/nucleolar rim in the brightfield channel. The vicinity was defined as the distance below the threshold of 0.5 μm, similarly to Poulet et al. (2017). The distance was measured using software FIJI/ImageJ. For FRET-APB, enhanced GFP (eGFP) was excited at 488 nm with an argon laser and mCherry at 561 nm with a helium laser. Photobleaching was performed using a 561-nm laser in five frames with 100% power on a model no. SP8 Confocal Microscope (Leica). FRET efficiency was calculated as described by Bleckmann et al. (2010). Subnuclear localization of candidate proteins in Arabidopsis was analyzed on 2-week–old seedlings of stable transgenic lines grown vertically on 1/2-strength Murashige and Skoog plates for conventional confocal microscopy and 6-d–old plants for AiryScan microscopy (Zeiss). Seedlings were transferred to the microscopic slides and cut around the hypocotyl, leaving the root on the slide. eGFP signals in roots were analysed using excitation at 488 nm with an argon laser. Images were acquired with 3- to 4-line averaging.

For superresolution imaging, the confocal laser scanning microscope model no. LSM880 (Zeiss) with AiryScan was used with a C-Apochromat 40×/1.2 Korr FCS M27 water immersion objective (Zeiss). The excitation wavelengths of 488 nm for eGFP and 561 nm for propidium iodide were used and emission was detected from 495 to 550 nm and 570 to 620 nm, respectively. The super-resolution mode of the AiryScan detector was used for acquisition at a pixel size of 0.04 μm and the processing of the acquired raw images was done using the standard 2D AiryScan filtering (Wiener filter associated with deconvolution at "auto") in the software ZEN blue (Zeiss). Images from both channels were merged and only their brightness adjusted using the software ZEN blue. All samples from different tissues were treated the same during the processing.

Y2H

Yeast cultures were grown at 28°C on Yeast Peptone Dextrose (YPD) or on selective Synthetic Dextrose (SD) media. The AH109 strain was used for transformation, following protocol described in the Yeast Protocols Handbook (version no. PR973283 21; Clontech), with both Gal4-BD and Gal4-AD constructs added. Transformants were selected on SD medium lacking Trp and Leu (SD-LW). Protein interaction was assessed by transformant growth on selective, but low stringency SD media additionally lacking His (SD-LWH) permitting the identification of weak interactions (in Y2H).

Nuclear Morphology Analysis

For analysis, 0.5 g of 2-week-old seedlings were fixed in 10 mL of freshly prepared ice-cold 4 (w/v) % formaldehyde in PBS buffer for 20 min under vacuum. The seedlings were washed three times for 5 min in PBS buffer. After removal of PBS, the material was chopped on ice with a razor blade in 50 μL of Nuclear Isolation Buffer (NIB: 500 mM of Suc, 100 mM of KCl, 10 mM of Tris-HCl at pH 9.5, 10 mM of EDTA, 4 mM of spermidine, 1 mM of spermine, and 0.1% [v/v] Beta-mercaptoethanol). An additional 450 μL of NIB was added and cellular solution was filtered through 50-μm cell strainers (cat. no. 04-0042-2317; Partec). The filtrate was centrifuged at 500*g*, for 3 min, 4°C. The pellet was resuspended in 40 μL of NIB and 2 to 3 μL was spread on a microscopic slide, left to dry, and mixed subsequently with 4 μg/mL of DAPI solution (cat. no. 6335; Roth) in Vectashield mounting medium (cat. no. H-1000; Vector Laboratories). DAPI-stained nuclei were visualized in Z-stacks done on a model no. SP8 Confocal Microscope (Leica) using a 405-nm diode. Acquired Z-stacks were manually thresholded and used for nuclear shape and size measurements in the FIJI implementation of the software ImageJ2 (National Institutes of Health; Schindelin et al., 2012). Nuclear area and circularity index measurements were performed on *Z* plane showing the largest area of particular nucleus in the Z-stack. Circularity index was calculated as: 4π (area/perimeter^2), with a maximal value of 1.0 corresponding to the perfect circle. The measurements were done on 72 to 92 nuclei per genotype. Significance was calculated using one-way analysis of variance and Student's *t* test.

Ploidy Analyses

Ploidy analyses were performed with 10-d–old whole seedlings (eight seedlings per sample) and cotyledons (12 per sample). Tissue was chopped in nuclei isolation buffer (15 mM of Tris; 2 mM of Na2-EDTA; 0.5 mM of Spermine; 80 mM of KCL; 20 mM of NaCl; 15 mM of β-Mercaptoethanol; 0.1% Triton X-100, pH-adjusted to 7.5), filtered through a 50-μm mesh, stained with Propidium iodide (0.005 mg/mL) and the DNA content was measured using a Fluorescence Activated Cell Sorter (Aria; BD Bioscience). Cycle value, which represents the mean number of endoreduplication cycles per nucleus, was calculated as in Barow and Meister (2003).

Transcriptomics

RNA was extracted from 2-week–old seedlings using the RNeasy Plant Mini Kit (cat. No. 74904; Qiagen), according to the manufacturer's manual. RNA was treated with DNase and its quality was assessed on a Nanodrop 1000 (Thermo Fisher Scientific), by Qubit RNA BR Assay (cat. no. Q12210; Thermo Fisher Scientific) or using the RNA 6000 Nano Kit (cat. no. 5067-1511; Agilent) on a Bioanalyzer (cat. no. 2100; Agilent). First-strand cDNA was synthesized using the RevertAid First Strand cDNA Synthesis Kit (cat. no. K1622; Thermo Fisher Scientific) with oligo-d(T) primers, according to the manufacturer's manual. cDNA was used for library preparation and sequencing on a HiSeq 2000 (Illumina). Alternatively, cDNA was used for RT-qPCR with the KAPA SYBR FAST Master Mix (cat. no. KK4600; Kapa Biosystems) on an iQ5 Detection System (Bio-Rad). Expression levels were calculated by application of $\Delta\Delta^{Ct}$ method. Sequences of oligonucleotides are shown in Supplemental Table 2. All the transcriptomic analyses were done in three or five independent biological replicates for RNA-Seq or RT-qPCR samples, respectively.

RNA-Seq Analysis

2 × 90-bp paired-end raw sequencing reads were scored by quality, then cleaned and trimmed from 5′ and 3′ ends in the softwares Trimmomatic (v0.35; http://www.usadellab.org/cms/?page=trimmomatic) and FastQC (v0.10; https://www.bioinformatics.babraham.ac.uk/projects/fastqc/). Clean reads were aligned to The Arabidopsis Information Resource 10 (TAIR10) reference genome by the software TopHat (v2.0.12; https://ccb.jhu.edu/software/tophat/index.shtml) with mate inner distance (−r) = 20 bp, segment length = 30 bp, and minimal intron length (−i) = 20 bp, according to Trapnell et al. (2009). Alignment files were processed in two different pipelines: Cufflinks (Tuxedo protocol; Trapnell et al., 2013) and EdgeR (Robinson et al., 2010). Fragments-per-kilobase of transcript-per-million mapped reads values were calculated in Cufflinks v2.2.1 with enabled: reference annotation (−g), multi read correction (−u), fragment bias correction (−b), and minimal intron length set to 20 bp. Cufflinks output was used to create common transcript reference file in the software Cuffmerge (v2.2.1.0; part of the Cufflinks suite) and perform DEG analysis in the software Cuffdiff (v2.2.1; part of the Cufflinks suite) with multi-read correction and fragment bias correction. For EdgeR, mapped reads were transformed into counts using HTSeq (v0.6.1; https://htseq.readthedocs.io/en/release_0.11.1/) and used as input for EdgeR (v3.3; https://bioconductor.org/packages/release/bioc/html/edgeR.html). Features with <1 count per million reads were discarded. For remaining features, differential expression was computed with adjusted *P* values < 0.

05. DEG analysis in either of the pipelines concerned comparison between wild-type and mutant (*pwo1* or *crwn1/2*) samples. To ensure the stringency of the analysis, only those genes that were present in DEG lists from both pipelines were taken for subsequent steps. The top DEGs in *pwo1* were validated by RT-qPCR using five independent biological replicates (Supplemental Figure 7). The oligonucleotides used for the validation are depicted in Supplemental Table 2.Hierarchical clustering of the replicates (Supplemental Figure 8) was done based on the matrix containing "counts per million" values calculated in the software HTSeq. Features with <1 count per million reads were discarded. Heatmap with correlation between replicates was obtained in the software Heatmap3 (v1.1.1; https://www.rdocumentation.org/packages/heatmap3/versions/1.1.1) using default methods for distance computing and dendrogram reordering.

Secondary Bioinformatic Analyses

Gene ontology of DEGs was inferred from Singular Enrichment Analysis on the AgriGO server (Du et al., 2010). Statistical significance was calculated using the Fisher test with the Yekutieli adjustment method and the threshold of $FDR < 0.01$ was applied. Arabidopsis TAIR10 genes were used as a reference.

For cross-comparison of DEGs in different mutant backgrounds, Venn diagrams were created in the software VENNY v2.1 (Oliveros, 2007). Statistical significance of overlapping gene number was calculated in the software "R" using the hypergeometric test. The total number of genes was set according to TAIR10 annotation (protein coding genes exclusively). The total number of proteins was set according to TAIR8 annotation, as the same reference was used for peptide annotation in MS analysis.

Accession Numbers

Sequence data from this article can be found in EMBL/GenBank data libraries under the accession numbers at3g03140 (PWO1), at2g23380 (CLF), at4g02020 (SWN), at1g67230 (CRWN1), at1g13220 (CRWN2), at5g65770 (CRWN4), at5g04990 (SUN1). RNA-Seq data (raw reads and a processed file) were deposited in the Gene Omnibus under series number GSE106615.

Supplemental Data

Supplemental Figure 1. Z-stack montage of PWO1-GFP localization to speckles in *N. benthamiana*.

Supplemental Figure 2. Subcellular localization of different constructs' combinations used for FRET-APB.

Supplemental Figure 3. PWO1 multiple alignment.

Supplemental Figure 4. Ploidy levels in *pwo1*.

Supplemental Figure 5. CRWN1 localization in *pwo1/3*.

Supplemental Figure 6. PWO1 localization in *crwn1*.

Supplemental Figure 7. RT-qPCR validation of RNA-Seq data for selected DEGs.

Supplemental Figure 8. Hierarchical clustering between samples in RNA-seq experiment.

Supplemental Table 1. List of PWO1 putative interactors.

Supplemental Table 2. Oligonucleotides for qPCR used in the study.

ACKNOWLEDGMENTS

We thank Dr. Eric Richards (Boyce Thompson Institute, Ithaca, NY) for sharing *crwn* mutants and CRWN1-GFP lines, Dr. Ruediger Simon (Heinrich Heine University Düsseldorf, Germany) for providing FRET vectors, and Keygene N.V. (Wageningen, Netherlands) for the training in RNA-Seq analysis. AiryScan imaging (Zeiss) was performed at the Center of Advanced Imaging, Heinrich Heine University Düsseldorf. We thank Dr. Julia Kleinmanns, Dorota Komar, and Dr. Suraj Jamge for critical revision of the article. This work was supported by the German Academic Exchange Service (Deutsche Akademische Austauschdienst Dienst; grant to Kalyanikrishna), the European Commission 7th FP Project (ITN Epi-TRAITS), the Boehringer Ingelheim Foundation (PLUS3 Program), the Deutsches Forschungsgemeinschaft (CRC973), and European Cooperation in Science & Technology COST Action (INDEPTH CA16212).

AUTHOR CONTRIBUTIONS

P.M., S.F., M.H., and D.S. designed the research; D.S., K.K., G.A., and M.H. designed the CoIP-MS/MS experiment; M.H. performed the CoIP-MS/MS experiment; C.S. analyzed MS spectral data; P.M., M.H., and K. performed nuclear morphology measurements; P.M. and S.F. performed microscopy analyses on PWO1 subnuclear localization in *N. benthamiana* and FRET analyses; P.M. did Y2H experiments, genetic interaction studies, subnuclear localization in Arabidopsis analyses, and transcriptomic experiments; Y.S. carried out superresolution imaging; P.M. wrote the article; D.S. and S.F. revised the article.

Received September 6, 2018; revised February 27, 2019; accepted March 22, 2019; published March 26, 2019.

REFERENCES

Atchison, L., Ghias, A., Wilkinson, F., Bonini, N., and Atchison, M.L. (2003). Transcription factor YY1 functions as a PcG protein in vivo. EMBO J. **22:** 1347–1358.

Barow, M., and Meister, A. (2003). Endopolyploidy in seed plants is differently correlated to systematics, organ, life strategy and genome size. Plant Cell Environ. **26:** 571–584.

Berry, S., Rosa, S., Howard, M., Bühler, M., and Dean, C. (2017). Disruption of an RNA-binding hinge region abolishes LHP1-mediated epigenetic repression. Genes Dev. **31:** 2115–2120.

Bi, X., Cheng, Y.J., Hu, B., Ma, X., Wu, R., Wang, J.W., and Liu, C. (2017). Nonrandom domain organization of the *Arabidopsis* genome at the nuclear periphery. Genome Res. **27:** 1162–1173.

Bieluszewski, T., Galganski, L., Sura, W., Bieluszewska, A., Abram, M., Ludwikow, A., Ziolkowski, P.A., and Sadowski, J. (2015). AtEAF1 is a potential platform protein for Arabidopsis NuA4 acetyltransferase complex. BMC Plant Biol. **15:** 75.

Bleckmann, A., Weidtkamp-Peters, S., Seidel, C.A., and Simon, R. (2010). Stem cell signaling in Arabidopsis requires CRN to localize CLV2 to the plasma membrane. Plant Physiol. **152:** 166–176.

Calonje, M., Sanchez, R., Chen, L., and Sung, Z.R. (2008). EMBRYONIC FLOWER1 participates in polycomb group-mediated AG gene silencing in Arabidopsis. Plant Cell **20:** 277–291.

Cesarini, E., et al. (2015) Lamin A/C sustains PcG protein architecture, maintaining transcriptional repression at target genes. J. Cell Biol. **211:** 533–551.

Ciska, M., and Moreno Díaz de la Espina, S. (2014). The intriguing plant nuclear lamina. Front. Plant Sci. **5:** 166.

Ciska, M., Masuda, K., and Moreno Díaz de la Espina, S. (2013). Lamin-like analogues in plants: The characterization of NMCP1 in *Allium cepa*. J. Exp. Bot. **64:** 1553–1564.

Cox, J., and Mann, M. (2008). MaxQuant enables high peptide identification rates, individualized p.p.b.-range mass accuracies and proteome-wide protein quantification. Nat. Biotechnol. **26:** 1367–1372.

Cox, J., Neuhauser, N., Michalski, A., Scheltema, R.A., Olsen, J.V., and Mann, M. (2011). Andromeda: A peptide search engine integrated into the MaxQuant environment. J. Proteome Res. **10:** 1794–1805.

Dechat, T., Adam, S.A., Taimen, P., Shimi, T., and Goldman, R.D. (2010). Nuclear lamins. Cold Spring Harb. Perspect. Biol. **2:** a000547.

Derkacheva, M., and Hennig, L. (2014). Variations on a theme: Polycomb group proteins in plants. J. Exp. Bot. **65:** 2769–2784.

Dittmer, T.A., Stacey, N.J., Sugimoto-Shirasu, K., and Richards, E.J. (2007). LITTLE NUCLEI genes affecting nuclear morphology in *Arabidopsis thaliana*. Plant Cell **19:** 2793–2803.

Du, Z., Zhou, X., Ling, Y., Zhang, Z., and Su, Z. (2010). agriGO: A GO analysis toolkit for the agricultural community. Nucleic Acids Res. **38:** W64-W70.

Fransz, P., De Jong, J.H., Lysak, M., Castiglione, M.R., and Schubert, I. (2002). Interphase chromosomes in Arabidopsis are organized as well defined chromocenters from which euchromatin loops emanate. Proc. Natl. Acad. Sci. USA **99:** 14584–14589.

Gardiner, J., Overall, R., and Marc, J. (2011). Putative Arabidopsis homologues of metazoan coiled-coil cytoskeletal proteins. Cell Biol. Int. **35:** 767–774.

Gibcus, J.H., and Dekker, J. (2013). The hierarchy of the 3D genome. Mol. Cell **49:** 773–782.

Gonzalez-Sandoval, A., Towbin, B.D., Kalck, V., Cabianca, D.S., Gaidatzis, D., Hauer, M.H., Geng, L., Wang, L., Yang, T., Wang, X., Zhao, K., and Gasser, S.M. (2015). Perinuclear anchoring of H3K9-methylated chromatin stabilizes induced cell fate in *C. elegans* embryos. Cell **163:** 1333–1347.

Gordon, M.R., Pope, B.D., Sima, J., and Gilbert, D.M. (2015). Many paths lead chromatin to the nuclear periphery. BioEssays **37:** 862–866.

Goto, C., Tamura, K., Fukao, Y., Shimada, T., and Hara-Nishimura, I. (2014). The novel nuclear envelope protein KAKU4 modulates nuclear morphology in Arabidopsis. Plant Cell **26:** 2143–2155.

Graumann, K. (2014). Evidence for LINC1-SUN associations at the plant nuclear periphery. PLoS One **9:** e93406.

Grob, S., Schmid, M.W., and Grossniklaus, U. (2014). Hi-C analysis in Arabidopsis identifies the KNOT, a structure with similarities to the flamenco locus of Drosophila. Mol. Cell **55:** 678–693.

Harr, J.C., Gonzalez-Sandoval, A., and Gasser, S.M. (2016). Histones and histone modifications in perinuclear chromatin anchoring: from yeast to man. EMBO Rep. **17:** 139–155.

Hennig, L., and Derkacheva, M. (2009). Diversity of Polycomb group complexes in plants: Same rules, different players? Trends Genet. **25:** 414–423.

Hernández-Muñoz, I., Taghavi, P., Kuijl, C., Neefjes, J., and van Lohuizen, M. (2005). Association of BMI1 with polycomb bodies is dynamic and requires PRC2/EZH2 and the maintenance DNA methyltransferase DNMT1. Mol. Cell. Biol. **25:** 11047–11058.

Hickman, M.A., Froyd, C.A., and Rusche, L.N. (2011). Reinventing heterochromatin in budding yeasts: Sir2 and the origin recognition complex take center stage. Eukaryot. Cell **10:** 1183–1192.

Hohenstatt, M.L., Mikulski, P., Komarynets, O., Klose, C., Kycia, I., Jeltsch, A., Farrona, S., and Schubert, D. (2018). PWWP-DOMAIN INTERACTOR OF POLYCOMBS11 interacts with Polycomb-group proteins and histones and regulates Arabidopsis flowering and development. Plant Cell **30:** 117–133.

Kadauke, S., and Blobel, G.A. (2009). Chromatin loops in gene regulation. Biochim. Biophys. Acta **1789:** 17–25.

Lai, Z., Schluttenhofer, C.M., Bhide, K., Shreve, J., Thimmapuram, J., Lee, S.Y., Yun, D.J., and Mengiste, T. (2014). MED18 interaction with distinct transcription factors regulates multiple plant functions. Nat. Commun. **5:** 3064.

Libault, M., Tessadori, F., Germann, S., Snijder, B., Fransz, P., and Gaudin, V. (2005). The Arabidopsis LHP1 protein is a component of euchromatin. Planta **222:** 910–925.

Lichter, P., Cremer, T., Borden, J., Manuelidis, L., and Ward, D.C. (1988). Delineation of individual human chromosomes in metaphase and interphase cells by in situ suppression hybridization using recombinant DNA libraries. Hum. Genet. **80:** 224–234.

Margueron, R., and Reinberg, D. (2011). The Polycomb complex PRC2 and its mark in life. Nature **469:** 343–349.

Masuda, K., Xu, Z.-J., Takahashi, S., Ito, A., Ono, M., Nomura, K., and Inoue, M. (1997). Peripheral framework of carrot cell nucleus contains a novel protein predicted to exhibit a long α-helical domain. Exp. Cell Res. **232:** 173–181.

Mathieu, O., Probst, A.V., and Paszkowski, J. (2005). Distinct regulation of histone H3 methylation at lysines 27 and 9 by CpG methylation in Arabidopsis. EMBO J. **24:** 2783–2791.

Meuleman, W., Peric-Hupkes, D., Kind, J., Beaudry, J.-B., Pagie, L., Kellis, M., Reinders, M., Wessels, L., and van Steensel, B. (2013). Constitutive nuclear lamina-genome interactions are highly conserved and associated with A/T-rich sequence. Genome Res. **23:** 270–280.

Oh, S., Park, S., and van Nocker, S. (2008). Genic and global functions for Paf1C in chromatin modification and gene expression in Arabidopsis. PLoS Genet. **4:** e1000077.

Oliveros, J.C. (2007). VENNY. An interactive tool for comparing lists with Venn Diagrams. http://bioinfogp.cnb.csic.es/tools/venny/index.html.

Ozawa, R., Hayashi, Y.K., Ogawa, M., Kurokawa, R., Matsumoto, H., Noguchi, S., Nonaka, I., and Nishino, I. (2006). Emerin-lacking mice show minimal motor and cardiac dysfunctions with nuclear-associated vacuoles. Am. J. Pathol. **168:** 907–917.

Pirrotta, V., and Li, H.-B. (2012). A view of nuclear Polycomb bodies. Curr. Opin. Genet. Dev. **22:** 101–109.

Poulet, A., Duc, C., Voisin, M., Desset, S., Tutois, S., Vanrobays, E., Benoit, M., Evans, D.E., Probst, A.V., and Tatout, C. (2017). The LINC complex contributes to heterochromatin organisation and transcriptional gene silencing in plants. J. Cell Sci. **130:** 590–601.

Robinson, M.D., McCarthy, D.J., and Smyth, G.K. (2010). edgeR: a Bioconductor package for differential expression analysis of digital gene expression data. Bioinformatics **26:** 139–140.

Sakamoto, Y., and Takagi, S. (2013). LITTLE NUCLEI 1 and 4 regulate nuclear morphology in *Arabidopsis thaliana*. Plant Cell Physiol. **54:** 622–633.

Schindelin, J., et al. (2012) FIJI: An open-source platform for biological-image analysis. Nat. Methods **9:** 676–682.

Smaczniak, C., et al. (2012) Characterization of MADS-domain transcription factor complexes in Arabidopsis flower development. Proc. Natl. Acad. Sci. USA **109:** 1560–1565.

Taddei, A., Hediger, F., Neumann, F.R., Bauer, C., and Gasser, S.M. (2004). Separation of silencing from perinuclear anchoring functions in yeast Ku80, Sir4 and Esc1 proteins. EMBO J. **23:** 1301–1312.

Tan, L.-M., Zhang, C.-J., Hou, X.-M., Shao, C.-R., Lu, Y.-J., Zhou, J.-X., Li, Y.-Q., Li, L., Chen, S., and He, X.-J. (2018). The PEAT protein complexes are required for histone deacetylation and heterochromatin silencing. EMBO J. **37:** e98770.

Towbin, B.D., González-Aguilera, C., Sack, R., Gaidatzis, D., Kalck, V., Meister, P., Askjaer, P., and Gasser, S.M. (2012). Step-wise methylation of histone H3K9 positions heterochromatin at the nuclear periphery. Cell **150:** 934–947.

Trapnell, C., Pachter, L., and Salzberg, S.L. (2009). TopHat: discovering splice junctions with RNA-Seq. Bioinformatics **25:** 1105–1111.

Trapnell, C., Hendrickson, D.G., Sauvageau, M., Goff, L., Rinn, J.L., and Pachter, L. (2013). Differential analysis of gene regulation at transcript resolution with RNA-seq. Nat. Biotechnol. **31:** 46–53.

Van Bortle, K., and Corces, V.G. (2012). Nuclear organization and genome function. Annu. Rev. Cell Dev. Biol. **28:** 163–187.

van Steensel, B., and Belmont, A.S. (2017). Lamina-associated domains: Links with chromosome architecture, heterochromatin, and gene repression. Cell **169:** 780–791.

Vieux-Rochas, M., Fabre, P.J., Leleu, M., Duboule, D., and Noordermeer, D. (2015). Clustering of mammalian *Hox* genes with other H3K27me3 targets within an active nuclear domain. Proc. Natl. Acad. Sci. USA **112:** 4672–4677.

Wang, H., Dittmer, T.A., and Richards, E.J. (2013). Arabidopsis CROWDED NUCLEI (CRWN) proteins are required for nuclear size control and heterochromatin organization. BMC Plant Biol. **13:** 200.

Zhou, J.X., Liu, Z.W., Li, Y.Q., Li, L., Wang, B., Chen, S., and He, X.J. (2018). Arabidopsis PWWP domain proteins mediate H3K27 trimethylation on FLC and regulate flowering time. J. Integr. Plant Biol. **60:** 362–368.

Zhou, Y., Hartwig, B., James, G.V., Schneeberger, K., and Turck, F. (2016). Complementary activities of TELOMERE REPEAT BINDING proteins and Polycomb group complexes in transcriptional regulation of target genes. Plant Cell **28:** 87–101.